J Nanostruct 9(1): 146-153, Winter 2019

RESEARCH PAPER

A Novel Diethyl 2-(9-Fluorenyl) Malonate Functionlized SBA-15 for Selective Optical Sensing of Iron

Alireza Badiei [1,2] *, *Marzieh Yadavi* [1] *and Mehdi Karimi* [1]

[1] *School of Chemistry, College of Science, University of Tehran, Tehran, Iran*

[2] *Nanobiomedicine Centra of Excellence, Nanoscience and Nanotechnology Research Centra, University of Tehran, Tehran, Iran*

ARTICLE INFO

Article History:
Received 06 October 2018
Accepted 19 November 2018
Published 01 January 2019

Keywords:
Fe^{3+} ions chemosensor
Fluorene
Fluorescence
Mesoporous silica
SBA-15

ABSTRACT

In this study, highly ordered mesoporous silica material (SBA-15) functionalized with Diethyl 2 - (9 -fluorenyl) malonate as a flourophore is reported. The anchoring of flourophores to the hydroxyl group on SBA-15 surface was done with post synthesis method. The obtained materials were characterized by small and wide angle X-ray diffraction, N_2 adsorption–desorption, Fourier transform infrared spectroscopy and thermogravimetric analysis that indicate the successful immobilization of Diethyl 2 - (9 -fluorenyl) malonate on the surface of mesoporous silica. This organic–inorganic hybrid displayed highly selective and sensitive to Fe^{3+} ion over other cations such as Mg^{2+}, Cr^{3+}, Co^{2+}, Ni^{2+}, Cu^{2+}, Hg^{2+} and Zn^{2+}. Turn-off photoluminescence of this material was remarkably observed for iron ions in comparing of the other cations. A good linearity between the fluorescence intensity of the prepared material and the concentration of Fe^{3+} ion is constructed, which enables this martial as a fluorescence chemo sensor for detecting the Fe^{3+} ion with a suitable detection limit.

How to cite this article
Badiei A, Yadavi M and Karimi M. A Novel Diethyl 2-(9-Fluorenyl) Malonate Functionlized SBA-15 for Selective Optical Sensing of Iron. J Nanostruct, 2019; 9(1):146-153. DOI: 10.22052/JNS.2019.01.016

INTRODUCTION

The synthesis and modification of mesoporous silica have recently received much attention, due to its large surface area and pore volume, tunable and narrowly distributed pore diameter, controllable surface functionalization, chemical inertness, and biocompatibility, all of which have made it ideal inorganic matrix for use in adsorption, ion exchange, catalysis and sensing fields [1-3].

Iron is one of the most important elements in the biological systems, playing a significant role in the oxygen transport, storage and in the electron transport [4]. Regarding its industrial use, iron and its compounds have numerous important applications. However, despite the urgent need for iron-selective sensors for the potentiometric monitoring of Fe^{+3} ions in chemical, biological, industrial and environmental samples, there have been only limited reports of such solid-state electrochemiluminescence sensor in the literature [5, 6]. The need for determination of iron in clinical, medicinal, environmental and industrial samples has, the one hand, led to a number of methods for its measurement [7]. Previously, we reported the fluorene functionalized mesoporous silica based on mono, di and tri ammonium functionalized SBA-15 and studied its flourescence behavior in presence H^+ and Fe^{3+} [8, 9]. Also reported the synthesis of the fluorene functionalized mesoporous silica based on bis (2-aminoethyl)-2-(9-fluorenyl) malonamide to identify iron ion [10].

* *Corresponding Author Email: abadiei@khayam.ut.ac.ir*

Herein, fabrication of Fe^{3+}-optical sensor based on SBA-15 and Diethyl 2 - (9 -fluorenyl) malonate that functions as a flourophore in aqueous solution. In view of high chemical stability and fluorescent emission of fluorenyl, first we linked it as fluorophore to the dioxotetramine receptor then, to the 3-aminopropyltriethoxysilane and finally to the inner surface of mesoporous support SBA-15. In the presence of Fe^{3+}, this sensor shows highly selective and sensitive recognition toward Fe^{3+} over a wide range of tested cations including Mg^{2+}, Cr^{3+}, Co^{2+}, Ni^{2+}, Cu^{2+}, Hg^{2+} and Zn^{2+} without fluorescence intensity change. Compared with other reported fluorescent chemosensors for Fe^{3+} ions, this system showed the highest selectivity toward Fe^{3+} ions in aqueous solution.

MATERIALS AND METHODSS

Materials

$EO_{20}PO_{70}EO_{20}$ (P123, MW= 5800) was obtained from Aldrich. Fluorene, bromine, carbon tetrachloride, tetraethyl orthosilicate (TEOS), 3-aminopropyltriethoxysilane, Iron (II) sulfate, sodium carbonate, diethyl malonate and hydrochloric acid were obtained from Merck. . Iron (III) nitrate, magnesium nitrate, cupper (II) nitrate, cobalt (II) nitrate, nickel (II) nitrate, chromium (III) nitrate, mercury (II) nitrate and zinc nitrate were of analytical grade. Toluene and DMF were dried according to the standard purification methods [11].

Synthesis of SBA-15

SBA-15 material was prepared according to literature procedures [8, 10].

Synthesis of diethyl 2 - (9 -fluorenyl) malonate (Fm)

9-bromofluorene was prepared by literature methods [8, 12].The diethyl 2 -(9 -fluorenyl) malonate material was synthesized in accordance with the procedure reported by Luo et al [13]. To a solution of diethyl malonate (4.28 g, 0.027 mol) in anhydrous DMF (5 ml) were added Na_2CO_3 (2.83 g, 0.027 mol) and a solution of 9-bromofluorene (6.56 g, 0.027 mol) in DMF (20 ml) are added. The mixture was stirred at 70 °C for 24 h and subsequently poured into 250 ml ice water. The formed suspension was extracted three times with 25 ml portions of diethyl ether. The organic layer was dried over Na_2SO_4 and the solvent was removed by rotary evaporation to give a yellow solid (Fig. 1). After recrystallization from ethanol, yellow needle crystals were obtained; m.p. 69–72 °C, ν_{max} (cm^{-1}) 2977 (ν_{CH}), 1727 (ν_{CO}), 1447 and 1367 (ν_{CH}), 735 ($\nu_{C=C}$).

Sylilation of diethyl 2 - (9 -fluorenyl)malonate (Fm-Si)

The Fm-Si was synthesized based on ref [13]. The mixture of the diethyl 2 -(9 -fluorenyl) malonate (6.28 g, 0.001 mol) and 3-aminopropyltriethoxysilane (5 ml) was stirred at

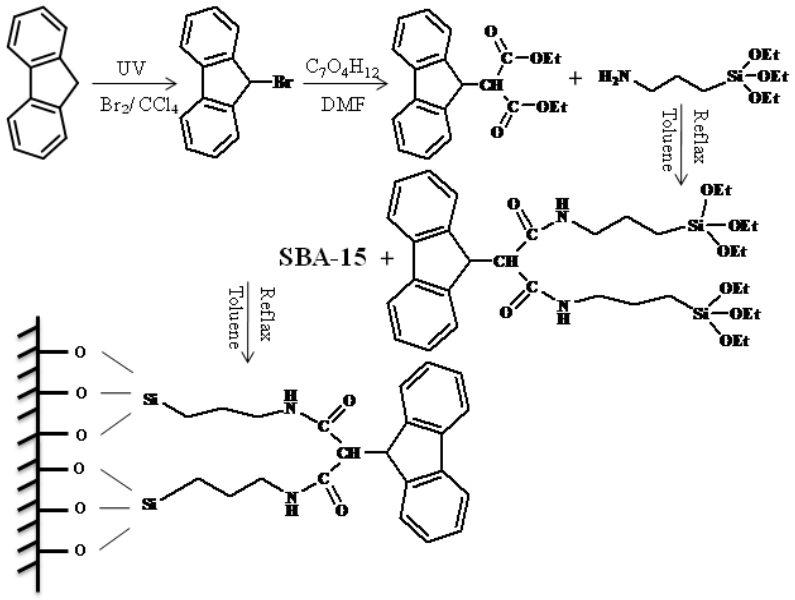

Fig. 1. Preparation of SBA-Fm-Si

35 °C for 72 h. Excess 3-aminopropyltriethoxysilane was distilled off under reduced pressure. After cooling, the yellow residue was treated and washed with diethyl ether ether (Scheme 1). ν_{max} (cm^{-1}) 2971 (ν_{CH}),1740 (ν_{CO}), 1446 (ν_{NH}), 1049 (ν_{SiO}) and 786 ($\nu_{C=C}$).

Synthesis of fluorene functionalized SBA-15 (SBA-Fm-Si)

0.1 g of SBA-15 was placed in a vacuum for 30 min, then 20 mL of dry toluene was added and stirred for 15 min. afterwards the Fm-Si (0.1 g, 0.285 mmol) was added to the resulting mixture under an inert atmosphere and refluxed for 24 h. Next, it was cooled at room temperature and the toluene was filtered and dried.

Instruments and spectroscopic measurements

Nitrogen physisorption isotherms were obtained on a BELSORP mini-II at liquid nitrogen temperature (77K). Surface area was measured using the Brunauer-Emmett-Teller (BET) method, pore size distributions were calculated from the nitrogen isotherms by Barrett-Joyner-Halenda (BJH) method. Small and wide angle x-ray scattering (SAXS) patterns were recorded with a model Hecus S3-MICROpix SAXS diffractometer with a one-dimensional PSD detector using Cu Kα radation (50KV, 1mA) at wave length 1.542 Å. FT-IR spectra were recorded a 4000-600 cm^{-1} region on Equinox 55 spectrometer. Thermogravimetric analysis (TGA) was performed on a TA Q50 instrument. The scans were performed between 20 °C and 900 °C at 10 °C/min. Emission spectra were recorded on Perkin-Elmer LS50 model luminescence spectrometer. Fluorescence measurements were done in a 1 cm quartz cuvette containing a magnetic-stirred solution of compounds in aqueous solvent (0.1g L^{-1}). Calcinations were carried out in a box furnace Gofa in the presence of flowing air. Melting points were determined by the capillary method on electro thermal 9100 apparatus.

RESULTS AND DISCUSSION

Small and wide angle X-ray diffraction

Fig. 2 shows X-ray diffraction patterns of SBA-15 and SBA-Fm-Si. Both samples have a single intense reflection around 2θ = 0.87° is characteristic of the long-range periodic in SBA-15 materials [14]. Two additional peaks around 2θ = 2° relate to the higher ordering (110) and (200) reflections, which are associated with a two-dimensional hexagonal (p6mm) structure [14]. However, the intensity of (100) reflection in SBA-Fm-Si is decreased due to the difference in the scattering contrast of the pores and the walls, and to the irregular coverage of organic groups on the nanochannels. The presence of those three reflections confirms that the hexagonal structure of the SBA-15 is preserved without collapsing during the modification of SBA-15 the surface. The larger wall thickness of SBA-Fm-Si is consistent with grafting the organic groups onto the pore walls. (Table1).

N_2 adsorption-desorption

Fig. 3 shows the N_2 adsorption-desorption isotherms of SBA-15 and SBA-Fm-Si. Both materials exhibit a typical irreversible type IV nitrogen adsorption isotherm with an H1 hysteresis loop as defined by IUPAC [14]. There is a shift of the hysteresis position toward low relative pressures and a slight decreasing trend in overall N_2 adsorption volume as the loading of Fm-Si groups. The pore size distribution was calculated from BJH method based on the desorption branch of the N_2 adsorption isotherm. As demonstrated in the inset of Fig. 3, a BJH plot of SBA- Fm-Si shows a narrow and uniform pore size distribution which is comparable to the original SBA-15, indicating that the integrity of the original structure of the SBA-15 was retained. In comparison with SBA-15 decreasment in the pore diameter value by about 1.4 nm is observed for SBA-Fm-Si. The textural parameters including specific surface areas (BET method), pore diameters (BJH method) and total

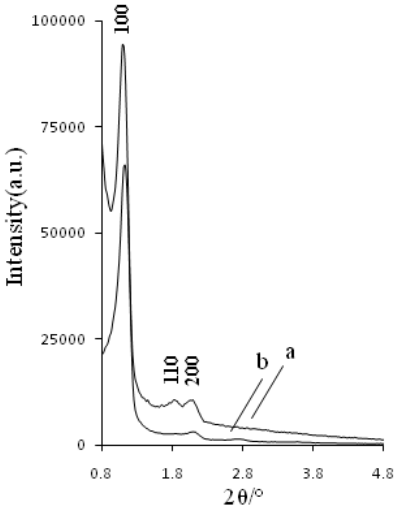

Fig. 2 Small angle XRD patterns a) SBA-15, b) SBA-Fm-Si

Table 1. Texture properties of prepared compounds [a]

Sample	D_{BJH} (nm)	S_{BET} ($m^2 g^{-1}$)	V_{total} ($cm^3 g^{-1}$)	w_t[b] (nm)	d_{100}(nm)
SBA-15	6.2	587	0.78	3.06	8.06
SBA-Fm-Si	4.8	237	0.39	4.65	7.78

[a] S_{BET} is the BET surface area; V is the total pore volume; D_{BJH} is the average pore diameter calculated using BJH method

[b] Wall thickness = $2/\sqrt{3}d_{(100)}$ − pore diameter

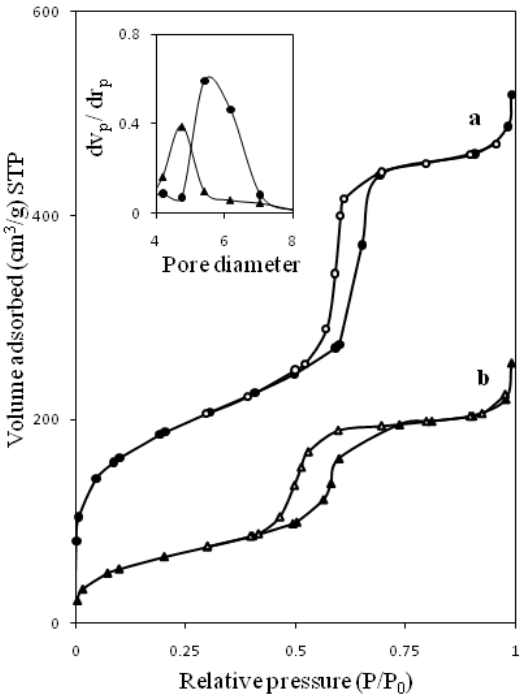

Fig. 3. N2 adsorption-desorption isotherms of a) SBA-15, b) SBA-Fm-Si (Inset: BJH pore size distribution curves of SBA-15 and SBA-Fm-Si)

pore volumes are given in Table 1. The decreasing of all three parameters in SBA-Fm-Si is due to the functionalization inside the channels of SBA-15.

Fig. 4 shows FT-IR spectra of SBA-15 and SBA-Fm-Si. The band at 3434 cm^{-1} in SBA-15 spectrum can be assigned to the stretching vibration of OH groups. The bands at 800 and 1086 cm^{-1} are attributed to Si-O-Si and Si-O stretching vibrations, respectively [15]. After grafting Fm-Si on the surface of SBA-15 in SBA-Fm-Si, the intensity of the band at 3434 cm^{-1} is decreased. The band at 2930 cm^{-1} is assigned to C-H stretching vibrations of the methylene groups. Moreover SBA-Fm-Si spectrum show the band at 1670 cm^{-1} which is the typical stretching frequency of the carbonyl in amid and the strong peak of 1450 cm^{-1} was observed which due to the C=C ring skeletal vibrations. These results indicated that the Fm-Si group was attached on the surface of SBA-15.

Fig. 5 gives the TGA profile of SBA-Fm-Si. The weight loss at around 100 °C corresponded to desorption of physisorbed water [16]. The weight loss 16.3 % at 180-600 °C is mainly due to the decomposition of Fm-Si groups in SBA-Fm-Si.

The fluorescence emission spectra of the suspension SBA-Fm-Si (200 µg/2.0 mL) in water exhibited two peaks at 310 nm and 410 nm (λ_{ex} = 260 nm) due to the grafted fluorene groups on the mesoporous silica (Fig. 7). The second emission could be observed between 360 nm to 410 nm for fluorene that depends on the media [17]. This emission is attributed to a novel kind of twisted intermolecular charge transfer (TICT) conformer within the life time of the lowest excited singlet state [18]. With the addition of Fe^{3+}, the emission peak intensity is significantly decreased. However no obvious changes could be observed upon the addition of Mg^{2+}, Cr^{3+}, Co^{2+}, Ni^{2+}, Cu^{2+}, Hg^{2+} and Zn^{2+} (Fig. 6).

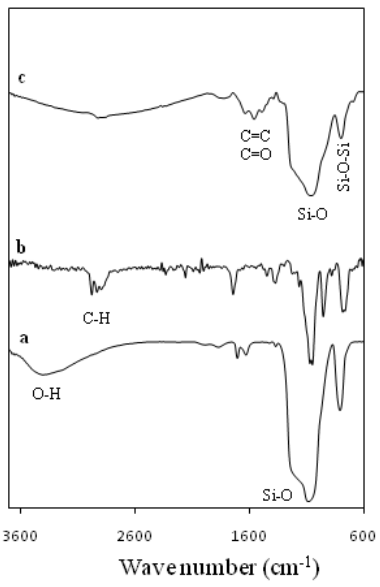

Fig. 4. FT-IR spectra of a) SBA-15, b) Fm-Si, c) SBA-Fm-Si

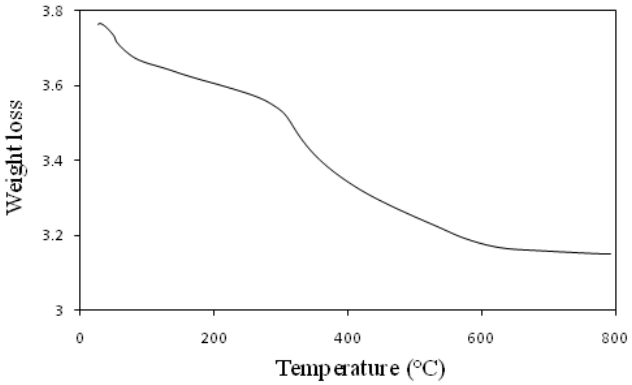

Fig. 5. TGA analysis of SBA-Fm-Si

These observations indicated that SBA-Fm-Si had a high sensitivity and excellent selectivity for Fe^{3+} in water. The results of fluorimetric titration indicate that fluorescence of fluorenyl was quenched by transfer of electron from metal center to photoexcited state of fluorenyl during coordination of Fe^{3+}. As shown in Fig. 7, a decrease of fluorescence intensity could be remarkably observed with an increasing Fe^{3+} concentration.

This high selectivity can be interpreted in terms of different charge density of metal ions. It is well known that the charge density (ρ) of a metal ion is defined as the amount of electric charge/ unit volume. It is one of the most important characterizations of the relative electrophilicity of a metal ion. The charge densities of metal ions were calculated according to the Eq. (1):

$$\rho = q/(4/3\pi r^3) \quad (1)$$

Where q is the formal charge and r denotes the Shannon ionic radius (Table 2) [19]. The calculated charge density of the cations are given in the table 2 and increased in the following order: Hg^{2+} (0.45) < Co^{2+} (1.15) < Zn^{2+} (1.18) < Cu^{2+} (1.22) < Mg^{2+} (1.28) < Ni^{2+} (1.45) < Cr^{3+} (3.08) < Fe^{3+} (6.09).

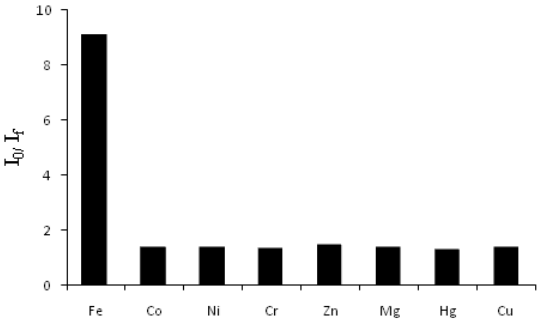

Fig. 6. Bar graphs of the fluorescence emission intensity for Fe^{3+}, Co^{2+}, Ni^{2+}, Cr^{3+}, Zn^{2+}, Mg^{2+}, Hg^{2+} and Cu^{2+} metal ions showing the metal ions selectivity profile of SBA-Fm-Si (200 μg/2.0 mL) with a concentration of 0.16 mM for each metal ion. I0 corresponds to emission of SBA-Fm-Si without metal ions.

The results indicate that the charge density of Fe^{3+} ion is the biggest among all of the competition ions. Therefore, the electrophilic ability of Fe^{3+} ion is the strongest among cations that can be used to interpret the capability of forming a coordination complex with an electron-rich ligand. Thus, the strong coordinate interaction between Fe^{3+} ions with the lone pair of the amine groups in SBA-Fm-Si significantly quench the fluorescence of fluorene because of the strong electrophilicity ability when it mixes with the other competition ions in the analytic solutions.

Fig. 8 shows the plot of $(I_0 - I)^{-1}$ vs. $[Fe^{3+}]^{-1}$, where I_0 and I refer to the emission fluorescence intensity at 310 nm for SBA-Fm-Si in the absence and presence of Fe^{3+} ions, respectively.

Generally, the mechanism of fluorescence quenching is divided into three types: dynamic quenching; static quenching; energy transfer [20]. Each of them is depicted through its special equation. A good linearity should be developed in the plot of $(I_0 - I)^{-1}$ vs. $[Fe^{3+}]^{-1}$ for the static quenching mechanism according to the following Line weaver-Burk equation (2) [21]:

$$(I_0 - I)^{-1} = I_0^{-1} + K_D (I_0 [Q])^{-1} \quad (2)$$

As it seen in Fig. 8, a good linearity between $(I_0 - I)^{-1}$ and the reciprocal of the concentration of Fe^{3+} from 0.16 to 0.83 mM (linearly dependent coefficient R^2 = 0.99) is constructed. According to the above equation, the dissociation constant K_D can be obtained from the slope and intercept of the line and the corresponding association

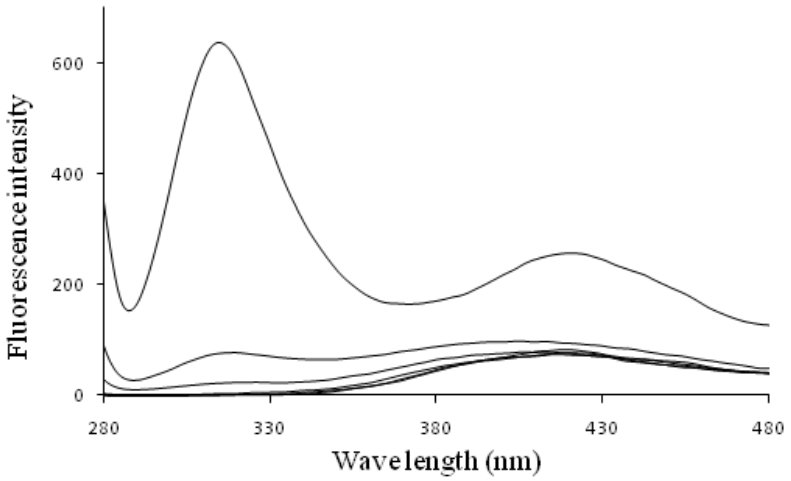

Fig. 7. Fluorescence emission spectra SBA-Fm-Si (0.1 g.L-1) in the presence of Fe^{3+} ions from 0.16 to 0.66 mM (λex = 260 nm)

Table 2. The charge densities and radius of metal ions

Element	Co^{+2}	Zn^{2+}	Mg^{2+}	Ni^{2+}	Cr^{3+}	Cu^{2+}	Hg^{2+}	Fe^{3+}
r	0.745	0.74	0.72	0.69	0.615	0.73	1.02	0.490
ρ	1.15	1.18	1.28	1.45	3.08	1.22	0.45	6.09

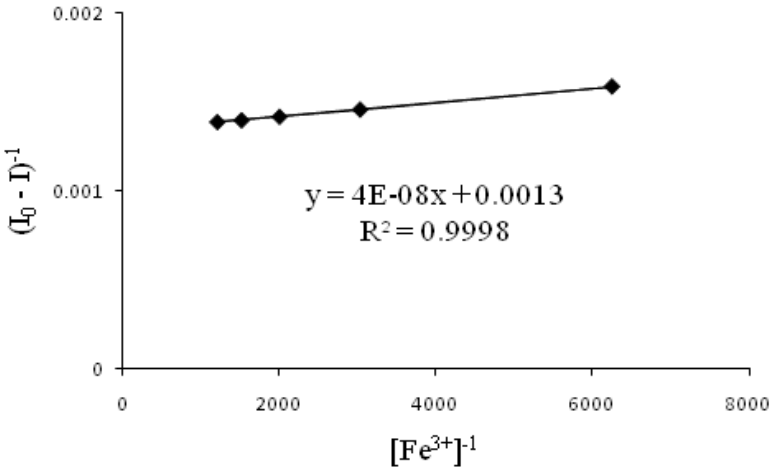

Fig. 8. Variation of (I0 - I)-1 of emission as a function of $[Fe^{3+}]$-1 for SBA-Fm-Si

Table 3. The detection limit and association constant

Sample	I_0^{-1}	$K_D I_0^{-1}$	K_D	K	S_D	m	DL
SBA-Fm-Si	0.0013	4×10^{-8}	3.08×10^{-5}	3.2×10^{4}	1.5	2.25×10^{5}	1.99×10^{-5}

constant K ($1/K_D$) is 3.2×10^4. Moreover the detection limit of SBA-Fm-Si for monitoring of Fe^{3+} are calculated according to Eq. (3), where DL is the minimal analytical signal that can be detected, S_D is the standard deviation of blank and m is the plot slope of fluorescence intensity vs. [Fe^{3+}].

$$DL = 3/S_D m \quad (3)$$

Therefore detection limit of SBA-Fm-Si was calculated to be 1.99×10^{-5}.

Based on consistent of fluorescence titration with the Line weaver-Burk equation, we could tentatively assign this quenching process as a static quenching mechanism that involves the interaction between the fluorescence molecule and the metal ions to form a nonfluorescent complex. This interaction often takes place in the ground state of the fluorescence molecule, and the quenching efficiency is governed by the formation constants and the concentration of metal ions [22].

CONCLUSION

We have introduced a selective and sensitive optical sensor to detect aqueous Fe^{3+} based on fluorene functionalized mesoporous silica. The materials were characterized using different techniques. Small and wide angle X-ray analysis showed that the mesoporous structure was preserved during process. N_2 adsorption-desorption isotherms display opening pores. Surface area and pore size were decreased by attaching the Fm-Si to the pore surface. FT-IR spectra demonstrated the incorporation of Fm-Si groups on the surface of SBA-15. Thermogravimetric analysis also indicates the successful immobilization of organic groups on to the surface of mesoporous silica. The sensing ability of SBA-Fm-Si was studied by fluorescence spectroscopy in presence of Fe^{3+}, Mg^{2+}, Cr^{3+}, Co^{2+}, Ni^{2+}, Cu^{2+}, Hg^{2+} and Zn^{2+}. In response to Fe^{3+}, the system provided remarkable fluorescence intensity change. Moreover, compared with the reported sensors for Fe^{3+} ions, this is the second chemosensor based on diethyl 2 -(9 -fluorenyl) malonate functionalized SBA-15 that can selectively detect Fe^{3+} in an aqueous environment. A good linearity between the fluorescence intensity of SBA-Fm-Si and the concentration of Fe^{3+} ion was observed, which enables this martial as a fluorescence chemosensor for detecting the Fe^{3+} ion with a suitable detection limit of 1.99×10^{-5}. We believe that the sensor can be promoted for a lot of sensible applications in chemical, environmental and biological systems.

ACKNOWLEDGMENTS

The authors wish to thank the University of Tehran for financially supporting this work.

CONFLICT OF INTEREST

The authors declare that there are no conflicts of interest regarding the publication of this manuscript.

REFERENCE

1. Kresge CT, Leonowicz ME, Roth WJ, Vartuli JC, Beck JS. Ordered mesoporous molecular sieves synthesized by a liquid-crystal template mechanism. Nature. 1992;359(6397):710-2.
2. Corma A. From Microporous to Mesoporous Molecular Sieve Materials and Their Use in Catalysis. Chemical Reviews. 1997;97(6):2373-420.
3. Sorensen AC, Fuller BL, Eklund AG, Landry CC. Mo-Doped Mesoporous Silica for Thiophene Hydrodesulfurization: Comparison of Materials and Methods. Chemistry of Materials. 2004;16(11):2157-64.
4. Greenwood NN, Earnshaw A. Preface. Chemistry of the Elements: Elsevier; 1984. p. v-vi.
5. Zhang X-B, Cheng G, Zhang W-J, Shen G-L, Yu R-Q. A fluorescent chemical sensor for Fe3+ based on blocking of intramolecular proton transfer of a quinazolinone derivative. Talanta. 2007;71(1):171-7.
6. Sahoo SK, Sharma D, Bera RK, Crisponi G, Callan JF. Iron(iii) selective molecular and supramolecular fluorescent probes. Chem Soc Rev. 2012;41(21):7195.
7. Arruda Fatibello SHS, Henriques Vieira AA, Fatibello-Filho O. A rapid spectrophotometric method for the determination of transparent exopolymer particles (TEP) in freshwater. Talanta. 2004;62(1):81-5.
8. Yadavi M, Badiei A, Ziarani GM. A novel Fe3+ ions chemosensor by covalent coupling fluorene onto the mono, di- and tri-ammonium functionalized nanoporous silica type SBA-15. Applied Surface Science. 2013;279:121-8.
9. Yadavi M, Badiei A, Ziarani G, Abbasi A. Synthesis of novel fluorene-functionalised nanoporous silica and its luminescence behaviour in acidic media. Chemical Papers. 2013;67(7).
10. Yadavi M, Badiei A. Turn-off Fluorescence Chemosensor for Iron with Bis(2-aminoethyl)-2-(9-fluorenyl)malonamide Functionlized SBA-15. Journal of Fluorescence. 2013;24(2):523-31.
11. Armarego WLF. Purification of Organic Chemicals. Purification of Laboratory Chemicals: Elsevier; 2017. p. 95-634.
12. Badiei A, Goldooz H, Ziarani GM. A novel method for preparation of 8-hydroxyquinoline functionalized mesoporous silica: Aluminum complexes and photoluminescence studies. Applied Surface Science. 2011;257(11):4912-8.
13. Jiang L-J, Luo Q-H, Duan C-y, Shen M-C, Hu H-W, Liu Y-J. A new dioxotetraamine ligand appended with fluorenyl and its copper(II) complex. Synthesis, crystal structure and solution behavior. Inorganica Chimica Acta.

1999;295(1):48-55.
14. Zhao D, Huo Q, Feng J, Chmelka BF, Stucky GD. Nonionic Triblock and Star Diblock Copolymer and Oligomeric Surfactant Syntheses of Highly Ordered, Hydrothermally Stable, Mesoporous Silica Structures. Journal of the American Chemical Society. 1998;120(24):6024-36.
15. Long DA. Infrared and Raman characteristic group frequencies. Tables and chartsGeorge Socrates John Wiley and Sons, Ltd, Chichester, Third Edition, 2001. Price £135. Journal of Raman Spectroscopy. 2004;35(10):905-.
16. Jaroniec CP, Kruk M, Jaroniec M, Sayari A. Tailoring Surface and Structural Properties of MCM-41 Silicas by Bonding Organosilanes. The Journal of Physical Chemistry B. 1998;102(28):5503-10.
17. Beltrán JL, Ferrer R, Guiteras J. Multivariate calibration of polycyclic aromatic hydrocarbon mixtures from excitation–emission fluorescence spectra. Analytica Chimica Acta. 1998;373(2-3):311-9.
18. Vogt BS, Schulman SG. Anomalous flourescence of 9-aminofluorene. Chemical Physics Letters. 1982;89(4):320-3.
19. Shannon RD. Revised effective ionic radii and systematic studies of interatomic distances in halides and chalcogenides. Acta Crystallographica Section A. 1976;32(5):751-67.
20. Lakowicz JR. Introduction to Fluorescence. Principles of Fluorescence Spectroscopy: Springer US; 1999. p. 1-23.
21. Di J, Yao K, Han W, Bi S. Study on the interaction of copper–zinc superoxide dismutase with aluminum ions by electrochemical and fluorescent method. Spectrochimica Acta Part A: Molecular and Biomolecular Spectroscopy. 2006;65(3-4):896-900.
22. De Costa MDP, Jayasinghe WAPA. Detailed studies on complexation behaviour and mechanism of fluorescence quenching of naphthalene linked hydroxamic acid with transition metal ions by UV-visible and fluorescence spectra. Journal of Photochemistry and Photobiology A: Chemistry. 2004;162(2-3):591-8.